Canonical perturbation theory for complex electron dynamics in gyrotron resonators

Y. Kominis
School of Electrical and Computer Engineering, National Technical University of Athens, Association EURATOM-Hellenic Republic, Zographou, GR-15773, Greece

O. Dumbrajs
Department of Engineering Physics and Mathematics, Helsinki University of Technology, Association EURATOM-TEKES, FIN-02150 Espoo, Finland and Institute of Solid State Physics, University of Latvia, Kengaraga Strasse 8, LV-1063, Riga, Latvia

K. A. Avramides, K. Hizanidis, and J. L. Vomvoridis
School of Electrical and Computer Engineering, National Technical University of Athens, Association EURATOM-Hellenic Republic, Zographou, GR-15773, Greece

(Received 6 July 2005; accepted 28 September 2005; published online 8 November 2005)

Complex electron dynamics in gyrotron resonators are analyzed in the context of the Hamiltonian formalism. Application of the canonical perturbation theory provides analytical approximate invariants of the electron motion. The latter are used for describing the resonant structure of the electron phase space and the electron rest energies at the output of the cavity. Hysteresis effects are also described through analytic expressions and approximate electron distribution functions are provided. The general case of resonant interaction at an arbitrary harmonic of the electron cyclotron frequency is considered and the effect of a varying frequency mismatch is studied. Also, the case of electron interaction with multiple rf modes is investigated. © *2005 American Institute of Physics*. [DOI: 10.1063/1.2125547]

I. INTRODUCTION

Gyrotrons are microwave devices, which are able to generate high-power, short-wavelength coherent radiation. Various technological applications[1] take advantage of the special features of gyrotrons, including radars, advanced communication systems, technological processes, extra-high-resolution spectroscopy, etc. Among them, one of the most important applications is the electron cyclotron resonance plasma heating in tokamaks.[2–4] Gyrotron operation is based on the stimulated cyclotron radiation of electrons oscillating in a static magnetic field and interacting with a rf mode in the gyrotron cavity. Although the physics of gyrotrons has been studied extensively,[5] the complex electron dynamics occurring under interaction with the rf field are still an issue of major interest. The dynamic process of electron motion in the gyrotron cavity possesses many features of chaotic dynamics. The latter induces the necessity of studying the impact of the electron motion complexity on (i) the spectrum of the electron residual energies after interaction with the rf field, the efficient operation of depressed collectors,[6] and (ii) the chaotic rf oscillations,[7] which appear under certain circumstances and can result in dramatic decrease of gyrotron efficiency and generation of other frequencies in addition to the desired one.

The electron motion, under the presence of a rf field, is described by a nonlinear dynamical system. This Hamiltonian system is, in general, nonintegrable. The rf field forms a "time-aperiodic" perturbation of the integrable free-electron motion, where the spatial longitudinal coordinate plays the role of "time." Although time-periodic (discrete spectrum) perturbations of Hamiltonian systems have been well studied[8] with the famous Kolmogorov–Arnold–Moser (KAM) theorem describing the generic features of such systems, the aperiodic perturbations (continuous spectrum) and the features of the corresponding dynamical systems are quite unexplored.

In this work we adopt the canonical perturbation method (CPM) as a unified analytical approach which is capable for (i) describing the complex phase-space dynamics through analytically obtained approximate invariants of the motion, (ii) providing analytical estimates for the electron residual energies at the output of the cavity, (iii) recovering successfully the hysteresis effects occurring in gyrotron resonators, and (iv) obtaining approximate solutions of the Vlasov equation, governing the evolution of the electron distribution function, which can also be used for calculating gyrotron efficiency, or other useful parameters of operation.

Chaotic electron trajectories have also been studied in previous works[9–12] for the case of interaction with a single rf mode being in resonance with the first harmonic of the electron cyclotron frequency. In this work we extend the application of the CPM in order to include the following cases: (i) a longitudinally varying frequency mismatch, due to the tapering of the magnetic field, which is widely used in certain gyrotron configurations and (ii) the realistic case of electron-beam interaction with multiple rf modes, being in resonance with the same or different harmonics of the electron cyclotron frequency. The latter results in resonance-overlap-like criteria[8,13] which are for the first time considered for aperiodic perturbation.

The aforementioned applicability of the CPM, both in the electron equations of motion and the Vlasov equation,

governing the evolution of the electron distribution function, and widely used in plasma physics, suggests this method as a unified context for studying electron dynamics in gyrotron resonators. Low-order calculations are shown to be in good agreement with numerical results; moreover, the method can be easily proceed to higher orders through the Lie transformation formalism.[14]

II. ELECTRON EQUATIONS OF MOTION

The electron motion under interaction with a set of rf modes is governed by the equation

$$\frac{dp}{d\zeta} + ip(|p|^2 - 1) = i\sum_s n_s F_s (p^*)^{n_s - 1} f_s(\zeta) e^{in_s \int_0^\zeta \Delta_s(\zeta')d\zeta'}, \quad (1)$$

where p is the dimensionless transverse momentum of the electron, $\zeta = (\beta_{\perp 0}^2 \omega_{c0}/2\beta_{\|0} c)z$ is the dimensionless coordinate, F_s is the normalized rf field amplitude, $f_s(\zeta)$ is the rf field profile of the sth mode, $\Delta_s(\zeta) = (2/\beta_{\perp 0}^2)[(\omega_s - n_s \omega_c/\omega_s)]$ is the frequency mismatch between the sth mode and the n_sth harmonic of the cyclotron frequency, $\omega_c = (e/m)B/\gamma_{\mathrm{rel}}$ is the electron cyclotron frequency, $\omega_{c0} = (e/m)B_0/\gamma_{\mathrm{rel}}$ is the electron cyclotron frequency at the entrance of the cavity, $\beta_{\perp 0} = v_{\perp 0}/c$, $\beta_{\|0} = v_{\|0}/c$ are the normalized transverse and parallel velocities of the electron at the entrance to the cavity, B is the magnetic field, $\gamma_{\mathrm{rel}} = 1 + (e/mc^2)U$ is the relativistic factor, and U is the accelerating voltage. For the purposes of the analysis of this work we use the transformation $p \to p \exp(-i\zeta)$, resulting in the equation

$$\frac{dp}{d\zeta} + ip|p|^2 = i\sum_s n_s F_s (p^*)^{n_s - 1} f_s(\zeta) e^{-in_s \int_0^\zeta \delta_s(\zeta')d\zeta'}, \quad (2)$$

where $\delta_s(\zeta) \equiv 1 - \Delta_s(\zeta)$. This form of the electron equations of motion results, in a constant sign of the frequency of oscillations for the free-electron motion, which, as will be seen in the following, is useful for the definition of the Poincaré surface of section on the phase space. By transforming to action-angle variables: $p = \sqrt{2J} e^{-i\theta}$ we obtain

$$\frac{dJ}{d\zeta} = -\sum_s n_s F_s (2J)^{n_s/2} \,\mathrm{Im}\{e^{in_s\theta} f_s(\zeta) e^{-in_s \int_0^\zeta \delta_s(\zeta')d\zeta'}\}, \quad (3)$$

$$\frac{d\theta}{d\zeta} = 2J - \sum_s n_s F_s (2J)^{n_s/2 - 1} \,\mathrm{Re}\{e^{in_s\theta} f_s(\zeta) e^{-in_s \int_0^\zeta \delta_s(\zeta')d\zeta'}\}. \quad (4)$$

The system has the following Hamiltonian:

$$H(J, \theta, \zeta) = J^2 - \sum_s F_s (2J)^{n_s/2} \,\mathrm{Re}\{e^{in_s\theta} g_s(\zeta)\}, \quad (5)$$

where $g_s(\zeta) = f_s(\zeta) e^{-in_s \int_0^\zeta \delta_s(\zeta')d\zeta'}$.

III. CANONICAL PERTURBATION METHOD

In order to study a nonintegrable system we can start from an integrable system which differs from the actual one in terms of a small parameter and consider the actual system as a perturbation of the integrable one (near integrable). In our case the unperturbed (integrable) system can be defined as the one which describes the electron motion in the absence of the rf field, with Hamiltonian H_0.

The Hamiltonian of the perturbed (near-integrable) system can be written in terms of the action-angle variables of the unperturbed system as follows:

$$H(J, \theta, \zeta) = H_0(J) + H_1(J, \theta, \zeta), \quad (6)$$

$$H_0(J) = J^2, \quad (7)$$

$$H_1(J, \theta, \zeta) = -\sum_s F_s (2J)^{n_s/2} \,\mathrm{Re}\{e^{in_s\theta} g_s(\zeta)\}. \quad (8)$$

The aperiodic dependence of the perturbation term on the time ζ results in a phase-space topology consisting of infinite cylinders $[(J, \theta, \zeta) \in \mathbb{R} \times \mathbb{T} \times \mathbb{R}]$ in contrast with the usual toroidal topology $[(J, \theta, \zeta) \in \mathbb{R} \times \mathbb{T}^2]$ resulting from time-periodic perturbations. In order to construct the KAM curves of the perturbed system, via the canonical perturbation theory, we use successively near-identity canonical transformations to transform the Hamiltonian to a normal form in which the θ and ζ dependences are pushed to higher-order terms with respect to the small parameter of the perturbation method. The procedure can be continued to any order, with utilization of Lie series techniques. However, as will be shown, even a first-order approximation is capable of providing accurate information about for the electron phase space and the distribution function.

Following a standard procedure,[8] we seek a transformation to new variables $(\bar{J}, \bar{\theta})$ for which the new Hamiltonian $\bar{H}$ is a function of the action $\bar{J}$ alone. The generating function of this transformation $S(\bar{J}, \theta)$ is expanded S and $\bar{H}$ in power series of a small parameter ϵ (in our case $\epsilon \equiv F$),

$$S = \bar{J}\theta + \epsilon S_1 + \cdots, \quad (9)$$

$$\bar{H} = \bar{H}_0 + \epsilon \bar{H}_1 + \cdots, \quad (10)$$

where the lowest-order term has been chosen to generate the identity transformation $J = \bar{J}$ and $\bar{\theta} = \theta$. The old action and angle can be also expressed as power series in ϵ,

$$J = \bar{J} + \epsilon \frac{\partial S_1(\bar{J}, \theta, \zeta)}{\partial \theta} + \cdots, \quad (11)$$

$$\bar{\theta} = \theta + \epsilon \frac{\partial S_1(\bar{J}, \theta, \zeta)}{\partial \bar{J}} + \cdots. \quad (12)$$

The new Hamiltonian is

$$\bar{H}(\bar{J}, \bar{\theta}, \zeta) = H(J, \theta, \zeta) + \frac{\partial S(\bar{J}, \theta, \zeta)}{\partial \zeta}. \quad (13)$$

In order to find $\bar{H}$ Eqs. (11) and (12) must be inverted to give the old variables in terms of the new. To order ϵ this can be done easily by evaluating the first-order generating function in terms of the new angle $[S_1(\bar{J}, \theta, \zeta) = S_1(\bar{J}, \bar{\theta}, \zeta) + O(\epsilon)]$.

$$J = \bar{J} + \epsilon \frac{\partial S_1(\bar{J}, \bar{\theta}, \zeta)}{\partial \bar{\theta}} + \cdots, \tag{14}$$

$$\theta = \bar{\theta} - \epsilon \frac{\partial S_1(\bar{J}, \bar{\theta}, \zeta)}{\partial \bar{J}} + \cdots. \tag{15}$$

Inserting these equations into (13) and equating like powers of ϵ, we have to zero order

$$\bar{H}_0 = H_0(\bar{J}) \tag{16}$$

and to first order

$$\bar{H}_1 = \frac{\partial S_1}{\partial \zeta} + \omega_\theta \frac{\partial S_1}{\partial \bar{\theta}} + H_1, \tag{17}$$

where $\omega_\theta = \partial H_0 / \partial J$.

The appropriate choice of $\bar{H}_1$ incorporates all the essential terms coming from H_1, which yield nonphysical expressions for the generating function (and the corresponding near-identity transformation), when integrated along unperturbed orbits. Such expressions may not respect the periodicity of the original system or may not remain bounded (for example, a constant term in H_1 would result in an S_1 which increases infinitely with ζ), so that the ordering of the perturbation method is destroyed. However, the specific form of H_1, in our case, does not result in such expressions, as will be shown, so that $\bar{H}_1$ can be set equal to zero. Thus, the first-order equation is written in the following form:

$$\frac{\partial S_1}{\partial \zeta} + \omega_\theta \frac{\partial S_1}{\partial \bar{\theta}} = -H_1 \tag{18}$$

and has the solution (Appendix A)

$$S_1 = \sum_s \mathrm{Re}\left\{ F_s (2J)^{n_s/2} e^{i n_s \theta} \int_{-\infty}^{\zeta} g_s(t) e^{i n_s \omega_\theta (t-\zeta)} dt \right\}. \tag{19}$$

This form of the solution holds for a wide class of functions $g_s(\zeta)$ (rf field profiles) and can be obtained when the function $g_s(\zeta)$ is known in the real or the Fourier space (Appendix A). Moreover, the solution can also be constructed when the rf field profile or its spectrum has been found numerically.

The approximate invariant of the motion $\bar{J}$ can be written, to first order, as

$$\bar{J} = J - \frac{\partial S_1(J, \theta, \zeta)}{\partial \theta}. \tag{20}$$

Appropriate contour plots of the approximate invariant $\bar{J}$ can represent Poincaré surfaces of section of the phase space of the system. The family of curves

$$\bar{J}(J, \theta = \theta_0, \zeta) = \mathrm{const} \tag{21}$$

approximates the surface of section $\Sigma^{\theta_0} = \{(J, \zeta) \in \mathbb{R} \times \mathbb{R} : \theta = \theta_0, d\theta/d\zeta > 0\}$.

Moreover, for the case of an electron beam, where all electrons have an initial action value J_0 and angle values uniformly distributed in $[0, 2\pi]$, the extreme values of electron action at a specific ζ_0 (usually at the output of the cavity, which can be set to infinity, for simplification of calculations) are given by the solution of equation

$$J_0 = J \pm \max_{\theta \in [0, 2\pi]} \left\{ \left| \frac{\partial S_1(J, \theta, \zeta_0)}{\partial \theta} \right| \right\}, \tag{22}$$

with respect to J.

A. Case A: Constant mismatch Δ_s

We consider a constant mismatch $\delta_s(\zeta) = \delta_s^{(0)}$ and a Gaussian rf profile, so that

$$g_s(\zeta) = e^{-\zeta^2/2\sigma_s^2} e^{-i n_s \delta_s^{(0)} \zeta}, \tag{23}$$

where σ_s is the characteristic width of the Gaussian. In this case the first-order generating function is

$$S_1 = \sum_s F_s (2J)^{n_s/2} e^{i n_s \theta} e^{-i n_s \omega_\theta \zeta} \int_{-\infty}^{\zeta} e^{-t^2/2\sigma_s^2} e^{i n_s (\omega_\theta - \delta_s^{(0)}) t} dt, \tag{24}$$

$$S_1 = \sqrt{\frac{\pi}{2}} \sum_s F_s \sigma_s (2J)^{n_s/2} e^{i n_s \theta} e^{-i n_s \omega_\theta \zeta} e^{-\{[\omega_\theta - \delta_s^{(0)}]^2 n_s^2 \sigma_s^2/2\}} \times \left(1 + \mathrm{erf}\left[\frac{\zeta - i n_s [\omega_\theta - \delta_s^{(0)}] \sigma_s^2}{\sigma_s \sqrt{2}} \right] \right). \tag{25}$$

B. Case B: Linearly varying mismatch Δ_s

For the case of a linearly varying mismatch $\delta_s(\zeta) = \delta_s^{(0)} + 2\delta_s^{(1)}\zeta$, we have

$$g_s(\zeta) = e^{-\zeta^2/2\sigma_s^2} e^{-i n_s [\delta_s^{(0)} \zeta + \delta_s^{(1)} \zeta^2]} \tag{26}$$

or

$$g_s(\zeta) = e^{-[\zeta^2/2\sigma_{s(\mathrm{eff})}^2]} e^{-i n_s \delta_s^{(0)} \zeta}, \tag{27}$$

where

$$\sigma_{s(\mathrm{eff})}^2 = [\sigma_s^{-2} + 2 i n_s \delta_s^{(1)}]^{-1} = \frac{\sigma^2}{1 + 4 n_s^2 [\delta_s^{(1)}]^2} - i \frac{2 n_s \delta_s^{(1)}}{1 + 4 n_s^2 [\delta_s^{(1)}]^2}. \tag{28}$$

Thus, for the case of a linearly varying mismatch the generating function can be obtained from the previous case, if we simply substitute $\sigma_s = \sigma_{s(\mathrm{eff})}$.

IV. APPROXIMATE SOLUTION OF THE VLASOV EQUATION

The Vlasov equation for the electron distribution function F is given by

$$\frac{\partial F}{\partial \zeta} + [F, H] = 0. \tag{29}$$

It is well known that, since the Vlasov equation is quasilinear, it can be solved by utilizing the method of characteristics. The equations of the characteristics are the Hamiltonian equations of the electron motion. For the case of an inte-

grable system any function of the invariants of the motion is a solution of the Vlasov equation. Since $\bar{J}$ (11) is an approximate invariant of the motion, an approximate solution of the Vlasov equation has the form

$$F(J,\theta,\zeta)=F(\bar{J}). \tag{30}$$

According to the canonical perturbation method, the equation of the canonical transformation can be written as

$$\bar{J}=J-\epsilon\Delta J(\bar{J},\theta,\zeta), \tag{31}$$

where

$$\Delta J(\bar{J},\theta,\zeta)=\frac{\partial S_1}{\partial\theta}(\bar{J},\theta,\zeta). \tag{32}$$

Using the Taylor expansion of ΔJ, we solve this equation with respect to $\bar{J}=\bar{J}(J,\theta,\zeta)$,

$$\bar{J}=J-\epsilon\left\{\Delta J(J,\theta,\zeta)+\frac{\partial[\Delta J(J,\theta,\zeta)]}{\partial J}[-\epsilon\Delta J(J,\theta,\zeta)]\right\} \tag{33}$$

or

$$\bar{J}=J-\epsilon\Delta J+\epsilon^2\frac{1}{2}\frac{\partial}{\partial J}(\Delta J)^2. \tag{34}$$

Thus, the approximate solution of (29) has the form

$$F(\bar{J})=F\left[J-\epsilon\Delta J+\epsilon^2\frac{1}{2}\frac{\partial}{\partial J}(\Delta J)^2\right], \tag{35}$$

and by Taylor expanding with respect to J, we obtain

$$F(J,\theta,\zeta)=F(J)+\frac{\partial F}{\partial J}\left[-\epsilon\Delta J+\epsilon^2\frac{1}{2}\frac{\partial}{\partial J}(\Delta J)^2\right]+\frac{1}{2}\frac{\partial^2 F}{\partial J^2}\left[-\epsilon\Delta J+\epsilon^2\frac{1}{2}\frac{\partial}{\partial J}(\Delta J)^2\right]^2+\cdots \tag{36}$$

or

$$F(J,\theta,\zeta)=F(J)-\epsilon\frac{\partial F}{\partial J}\Delta J+\epsilon^2\frac{1}{2}\frac{\partial}{\partial J}\left[(\Delta J)^2\frac{\partial F}{\partial J}\right]+O(\epsilon^3). \tag{37}$$

According to the causality condition (Appendix A), $\lim_{\zeta\to-\infty}\Delta J=0$ and therefore

$$\lim_{\zeta\to-\infty}F(J,\theta,\zeta)=F(J). \tag{38}$$

For an initial (at $\zeta=-\infty$) distribution $F_0(J)$ we have

$$F(J,\theta)=F_0(J) \tag{39}$$

and the approximate solution of the Vlasov equation for the initial distribution F_0 is

$$F(J,\theta,\zeta)=F_0(J)-\epsilon\frac{\partial F_0}{\partial J}\Delta J+\epsilon^2\frac{1}{2}\frac{\partial}{\partial J}\left[(\Delta J)^2\frac{\partial F_0}{\partial J}\right]+O(\epsilon^3). \tag{40}$$

Knowledge of the distribution function is very useful for the calculation of several quantities of interest for the gyrotron operation, such as the electron susceptibility or the efficiency for the general case of an electron beam with an initial spread of transverse momentum (action). The perpendicular efficiency is defined by the expression

$$\eta_\perp=\langle|p(\zeta_{\rm in})|^2-|p(\zeta_{\rm out})|^2\rangle_\theta=2\langle J(\zeta_{\rm in})-J(\zeta_{\rm out})\rangle_\theta. \tag{41}$$

The averaging over the angles can be calculated through the distribution function according to

$$\langle J(\zeta_{\rm in})-J(\zeta_{\rm out})\rangle_\theta=\left\langle\int_{-\infty}^{\infty}J[F_0(J,\zeta_{\rm in})-F(J,\theta,\zeta_{\rm out})]dJ\right\rangle_\theta. \tag{42}$$

By substituting the distribution function (40) and taking into account that the first-order term results in a zero value, when averaged over the angles, we obtain

$$\langle J(\zeta_{\rm in})-J(\zeta_{\rm out})\rangle_\theta=-\left\langle\int_{-\infty}^{\infty}J\frac{1}{2}\frac{\partial}{\partial J}\left[(\Delta J)^2\frac{\partial F_0}{\partial J}\right]dJ\right\rangle_\theta. \tag{43}$$

After integration by parts we have

$$\langle J(\zeta_{\rm in})-J(\zeta_{\rm out})\rangle_\theta=-\frac{1}{2}\int_{-\infty}^{\infty}F_0(J)\frac{\partial\langle(\Delta J)^2\rangle_\theta}{\partial J}dJ. \tag{44}$$

We can write ΔJ in the simpler form

$$\Delta J=\sum_s|A_s|e^{i(n_s\theta-\phi_s)}, \tag{45}$$

where

$$A_s=\sqrt{\frac{\pi}{2}}n_sF_s(2J)^{n_s/2}\,e^{-\{[\omega_\theta-\delta_s^{(0)}]^2n_s^2\sigma_{s,R}^2/2\}}i\sigma_s\times\left(1+\mathrm{erf}\left\{\frac{\zeta-in_s[\omega_\theta-\delta_s^{(0)}]\sigma_s^2}{\sigma_s\sqrt{2}}\right\}\right), \tag{46}$$

$$\phi_s=n_s\omega_\theta\zeta+\frac{[\omega_\theta-\delta_s^{(0)}]^2n_s^2\sigma_{s,I}^2}{2}-\arg(A_s), \tag{47}$$

and $\sigma_{s,R}^2=\mathrm{Re}\{\sigma_s^2\}$, $\sigma_{s,I}^2=\mathrm{Im}\{\sigma_s^2\}$, so that we obtain

$$\langle(\Delta J)^2\rangle_\theta=\frac{1}{2}\sum_s|A_s|^2+\sum_{\substack{i\neq j\\ n_i=n_j}}|A_i||A_j|\cos(\phi_i-\phi_j). \tag{48}$$

For the case of an electron beam with all electrons having the same initial action value J_0 we have

$$F_0(J)=\delta(J-J_0), \tag{49}$$

and we obtain

$$\langle J(\zeta_{\rm in})-J(\zeta_{\rm out})\rangle_\theta=-\frac{1}{2}\frac{\partial}{\partial J_0}\langle\Delta J(J_0)^2\rangle_\theta, \tag{50}$$

which is in agreement with Madey's theorem.[15]

If we substitute ΔJ, for the case of a single rf mode, we obtain a gyrotron efficiency

$$\eta_{\perp} = 2\pi F^2 |\sigma|^2 n^2 \, e^{-\sigma_R^2 n^2 \Delta_0^2} (2\sigma_R^2 n^2 \Delta_0 - n), \tag{51}$$

where $\Delta_0 = 1 - \delta^{(0)}$, and we have set $J_0 = 0.5$ and consider $\zeta_{\text{out}} \to \infty$, for simplicity of the resulting expression. The latter is in agreement with previous calculations.[16] For the case of beam interaction with multiple rf modes on the same harmonic, the second sum in (48) is zero for large ζ ($\zeta \to \infty$), for modes with constant mismatch. However, for the case of linearly varying mismatch this term results in a remaining ζ dependence even for large ζ,

$$\langle J(\zeta_{\text{in}}) - J(\zeta_{\text{out}}) \rangle_{\theta} \sim \sum_{\substack{i \neq j \\ n_i = n_j = n}} |A_i||A_j| \cos\left(\{\sigma_{i,I}^2 [\omega_{\theta} - \delta_i^{(0)}]^2 - \sigma_{j,I}^2 [\omega_{\theta} - \delta_j^{(0)}]^2\} \frac{n^2}{2} \zeta \right). \tag{52}$$

For the case of an electron beam with action (transverse momentum) spread around J_0, described by a distribution function $F_0(J)$, the quantity of interest is the electronic efficiency η_{el}. For an ideal beam with no momentum spread the electronic efficiency is related to the perpendicular efficiency as

$$\eta_{\text{el}} = \frac{\beta_{\perp 0}^2}{2(1 - \gamma_0^{-1})} \eta_{\perp}, \tag{53}$$

while for the case of initial transverse momentum (action) spread η_{el} can be calculated by averaging over the distribution of the initial action values.

V. RESULTS AND DISCUSSION

In this section, the analytical results, obtained previously, are applied in specific cases, in order to study electron dynamics under interaction with a one or more rf modes. In all cases the following rf profile is used:

$$f(\zeta) = e^{[-(2\zeta/\mu - \sqrt{3})^2]}, \tag{54}$$

where $\mu = \pi(\beta_{\perp 0}^2/\beta_{\|0}) L_G/\lambda_c$ is the dimensionless length of the resonator, with L_G being the length of the resonator midsection. In normalizations we have used an electron cyclotron frequency of Ref. 5, instead of the usual wave frequency,[16] in order to study simultaneous interactions at different harmonics. As a result the product $n_s \mu$ corresponds to μ of Ref. 18. The analytical results of the previous sections are applied for this profile by setting $\sigma = \mu/\sqrt{8}$ and $\zeta \to \zeta - \sqrt{3}\mu/2$.

A. Interaction with a single rf mode

The phase-space dynamics of electrons are studied using the Poincaré surface of section Σ^{θ_0}. In Figs. 1–3 the cases of interaction with a single rf mode are shown for resonance in the first three ($n = 1, 2, 3$) harmonics, respectively, where $F = 0.01$, $\mu = 15$, and $\Delta = 0.5$. In the absence of the rf field, the Poincaré surface of section consists of straight lines, since the action (transverse momentum) is a constant of the motion. The presence of a rf field results in a strongly inhomogeneous phase space. There is an area of strong interaction

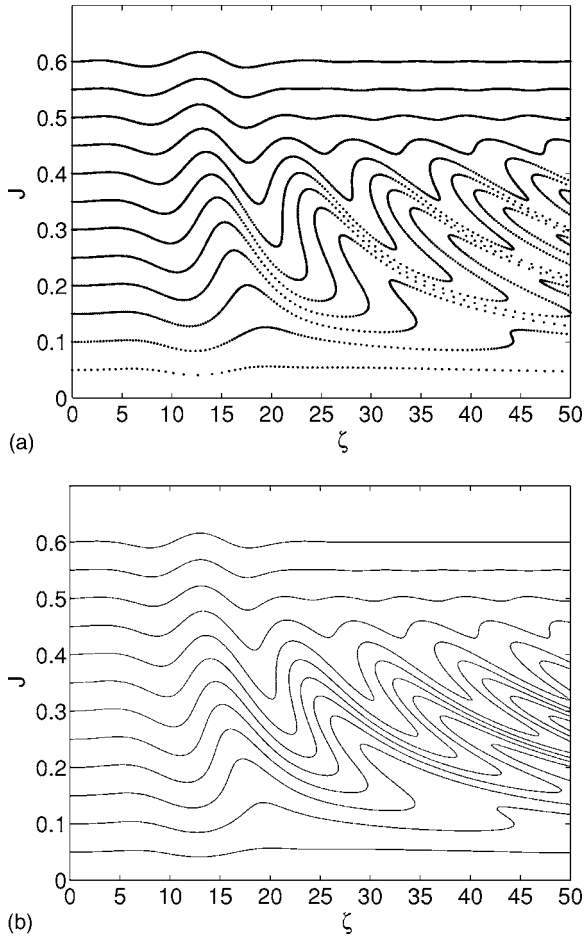

FIG. 1. (a) Numerically and (b) analytically [Eqs. (20) and (21)] obtained Poincaré surface of section $\Sigma^{\theta_0 = 0}$. Parameter set: $F = 0.01$, $\Delta = 0.5$, $\mu = 15$, $n = 1$.

which corresponds to a resonance between the frequency $\omega_{\theta} = 2J$ of electron rotation and the continuous spectrum of the effective perturbation $[g_s(\zeta)]$, which is centered at $\delta^{(0)}$ [Eqs. (23) and (26)]. For a constant mismatch Δ the resonant action value is $J_r = (1 - \Delta)/2$. It is obvious that interaction at higher harmonics results in weaker electron motion perturbation, and smaller resonant areas. For the numerically obtained Poincaré surfaces of section, the equations of motion have been solved for initial conditions consisted of a range of action (J) values and 101 uniformly distributed angle (θ) values in $[0, 2\pi]$, for each action value. The analytically obtained Poincaré surfaces of section have been constructed as contour plots of the approximate constant of the motion (21), and are shown in a remarkable agreement with the numerical results.

Higher values of F correspond in higher perturbation. In Figs. 4–6 a same (with Figs. 1–3) set of parameters has been used, except a higher value of the coupling factor $F = 0.1$. It is shown that analytical results are still in good qualitative agreement with the numerical results: the resonant structure of the phase space along with the width and the position of the resonant areas are well approximated. The latter are important for efficient gyrotron operation, since the action value of the electrons (electron beam) must correspond to the

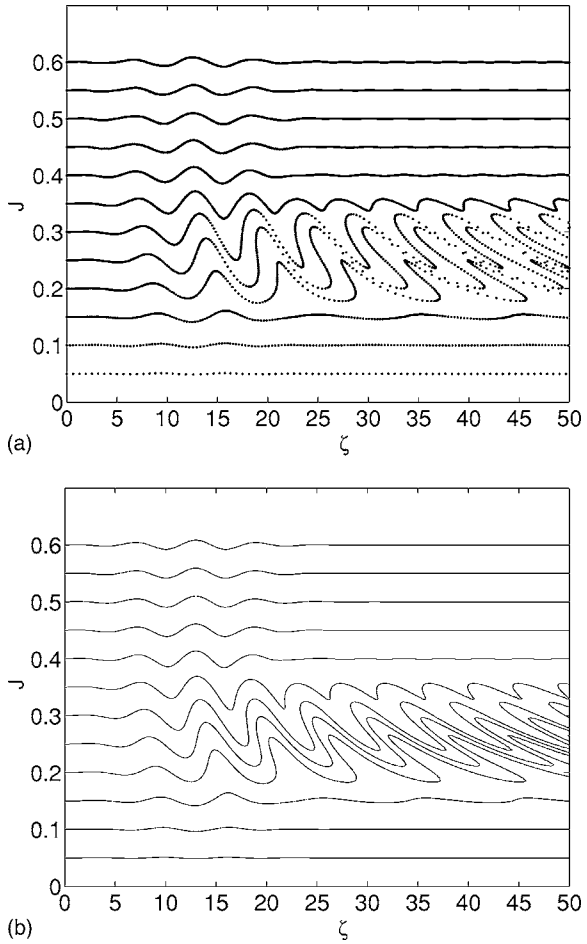

FIG. 2. (a) Numerically and (b) analytically [Eqs. (20) and (21)] obtained Poincaré surface of section $\Sigma^{\theta_0=0}$. Parameter set: $F=0.01$, $\Delta=0.5$, $\mu=15$, $n=2$.

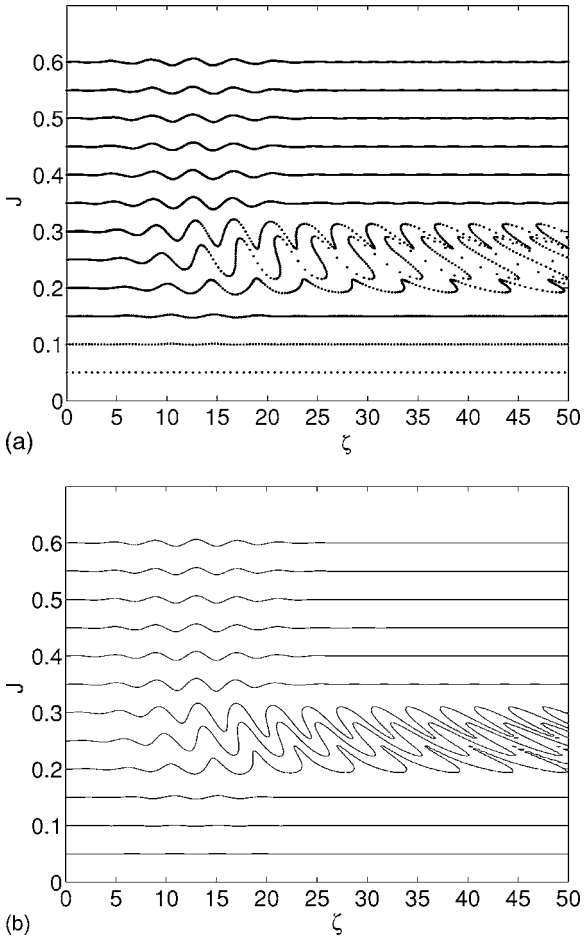

FIG. 3. (a) Numerically and (b) analytically [Eqs. (20) and (21)] obtained Poincaré surface of section $\Sigma^{\theta_0=0}$. Parameter set: $F=0.01$, $\Delta=0.5$, $\mu=15$, $n=3$.

upper bound of the resonant area, so that we have significant reduction of electron transverse momentum and thus energy transfer to the rf field.

As shown in Eq. (25), the width of the resonant area is inverse proportional to the product $n\sigma=n\mu/\sqrt{8}$, so that, in order to compensate for the width reduction of the resonant areas for resonances in higher harmonics (Figs. 1–3), shorter resonator lengths (μ) must be used. Also, from Eq. (25), it is shown that the amplitude of the generating function S_1 and, consequently, the effective perturbation is analogous to the product $F\sigma=F\mu/\sqrt{8}$. Thus, in order to increase the resonant area width while keeping the effective perturbation significantly large, we must consider smaller values of μ and larger values of F.

For the case of a varying frequency mismatch $\delta^{(1)}\neq 0$ the spectrum of the perturbation changes significantly. The effects of this spectral change on the electron dynamics are incorporated in the generating function S_1 and the corresponding approximate invariant of the motion. Thus, according to Eqs. (25) and (28) the effective resonator length [real part of $\sigma_{(\mathrm{eff})}$] is reduced by a factor $\{1+4n^2[\delta^{(1)}]^2\}^{-1}$, so that the width of the resonant area is increased, while the center of the resonant area is displaced, with respect to the case of constant mismatch, due to the imaginary part of $\sigma_{(\mathrm{eff})}$. Characteristic cases of varying frequency mismatch are shown in Figs. 7 and 8, for $n=1$ and $n=2$, respectively. In these cases we have considered negative values of $\delta^{(1)}$, corresponding to the configuration of a decreasing magnetic field $B_0(\zeta)$, for the case where the tapering of the magnetic field has been chosen according to the wall tapering $[B_0(\zeta)\sim 1/R(\zeta)]$, so that the cyclotron frequency (or its harmonic) is kept equal to the cutoff. Here it should be noted that the increase in the wall radius may significantly lower the diffractive Q factor of a resonator and may result in the necessity to take into account the changes in the electron axial momentum. This should be remembered in real designs of the resonators. However, it is remarkable that both equations for extreme action values at the output (22) and efficiency (51) are even functions of $\delta^{(1)}$, which coincides with the results of the ordinary linear theory of gyrotrons with a tapered magnetic field.[17] Since these equations result from first-order CPM, we can conclude that the effect of the sign of $\delta^{(1)}$ to the aforementioned quantities is of higher order.

The extreme action values at the output of the gyrotron resonator can be approximated by the solutions of Eq. (22). In Figs. 9(a) and 9(b), the maximum and minimum action values at the output are shown as a function of Δ, for an initial action value $J_0=0.5$. The values of Δ, at which the

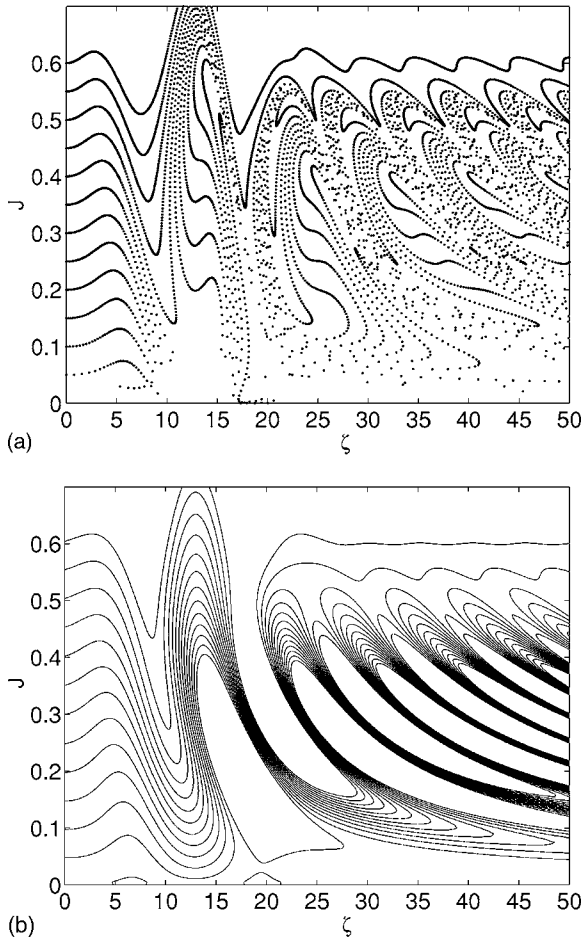

FIG. 4. (a) Numerically and (b) analytically [Eqs. (20) and (21)] obtained Poincaré surface of section $\Sigma^{\theta_0=0}$. Parameter set: $F=0.1$, $\Delta=0.5$, $\mu=15$, $n=1$.

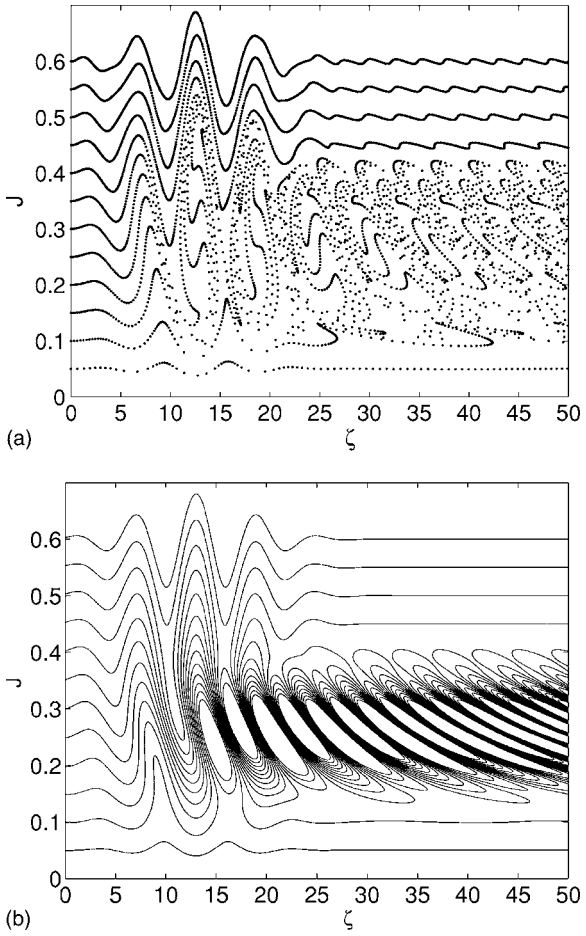

FIG. 5. (a) Numerically and (b) analytically [Eqs. (20) and (21)] obtained Poincaré surface of section $\Sigma^{\theta_0=0}$. Parameter set: $F=0.1$, $\Delta=0.5$, $\mu=15$, $n=2$.

extreme action values differ significantly from J_0, correspond to cases where J_0 resides inside the resonant area of the phase space. These diagrams summarize information for the electron energy spectrum. The effect of a varying frequency mismatch on the output electron spectrum is shown in Figs. 10(a) and 10(b) for the cases of resonance at the first ($n=1$) and second ($n=2$) harmonic. The widening of the resonant areas is due to the corresponding spectral widening of the perturbation (rf field) caused by the ζ dependence of the mismatch.

In order to obtain the curves of Figs. 9 and 10, Eq. (22) has been solved numerically by utilizing a standard Newton-Raphson method with initial value $J_0=0.5$. The sharp value transitions (depicted by dashed lines), occurring in some cases, are a result of the existence of more than one branch of solutions of Eq. (22) with respect to J. These cases are related to hysteresis effects which have been experimentally and numerically observed in gyrotron resonators for the case of slowly time-varying parameters.[18] For the case of resonance at the first harmonic $n=1$ and for a constant (in ζ) frequency mismatch $\delta^{(1)}=0$, Eq. (22) can be written in the following form:

$$J \pm \mu F \sqrt{\frac{\pi J}{2}} e^{-[(2J+\Delta-1)\mu/4]^2} = 0.5. \tag{55}$$

The solution of this equation has four branches

$$\Delta_{\text{left}}^{1,2} = \pm \frac{4}{\mu} \sqrt{-\ln A} - 2J + 1, \tag{56}$$

$$\Delta_{\text{right}}^{1,2} = \pm \frac{4}{\mu} \sqrt{-\ln(-A)} - 2J + 1, \tag{57}$$

where

$$A = \frac{0.5 - J}{\mu F \sqrt{\pi J/2}}. \tag{58}$$

These branches merge at the points $*$, as shown in Fig. 11. Their coordinates are given by the equations

$$\Delta_* = -\frac{\mu^2 F^2 \pi}{2} \pm \frac{\mu F \sqrt{\pi}}{2} \sqrt{4 + \mu^2 F^2 \pi}, \tag{59}$$

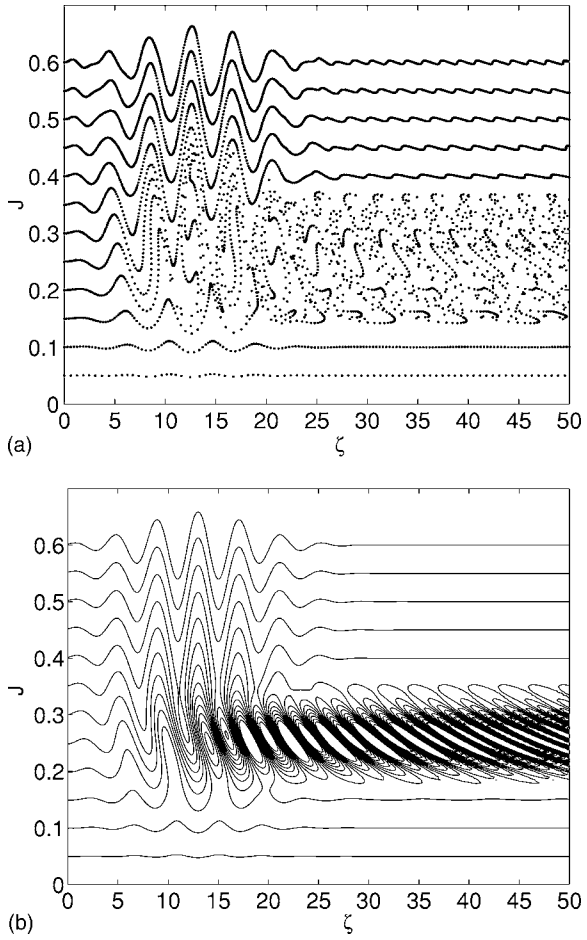

FIG. 6. (a) Numerically and (b) analytically [Eqs. (20) and (21)] obtained Poincaré surface of section $\Sigma^{\theta_0=0}$. Parameter set: $F=0.1$, $\Delta=0.5$, $\mu=15$, $n=3$.

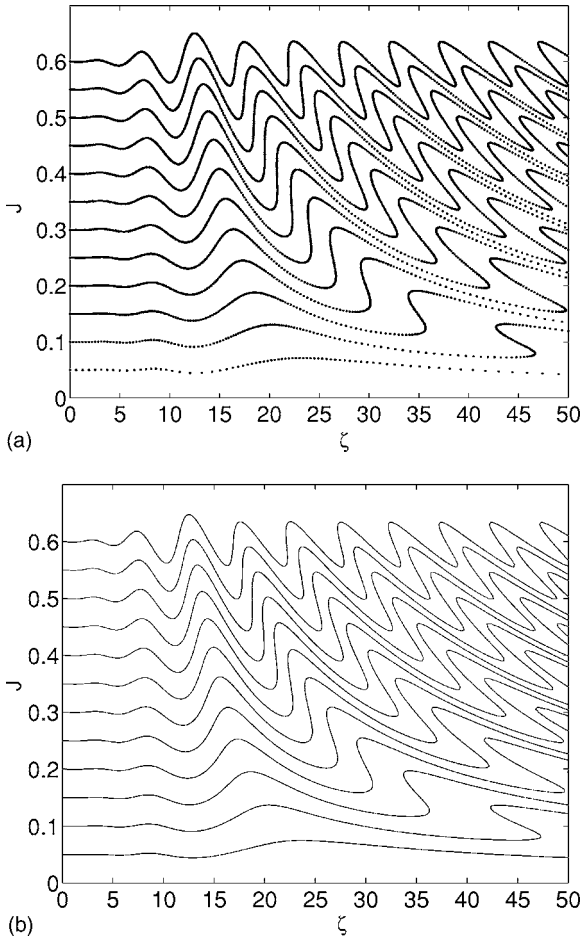

FIG. 7. Varying frequency mismatch. (a) Numerically and (b) analytically [Eqs. (20) and (21)] obtained Poincaré surface of section $\Sigma^{\theta_0=0}$. Parameter set: $F=0.01$, $\Delta=0.5$, $\mu=15$, $n=1$, $\delta^{(1)}=-0.05$.

$$J_* = \frac{2+\mu^2F^2\pi}{2} \pm \frac{\mu F\sqrt{\pi}}{2}\sqrt{4+\mu^2F^2\pi}. \tag{60}$$

These solutions do not merge at the points marked by o, but at $\pm\infty$, respectively. Points marked by ▲ and ▼ are hysteresis points, whose coordinates are determined by the equations

$$\frac{J_\blacktriangle + 0.5}{J_\blacktriangle - 2J_\blacktriangle^2} = -\mu\sqrt{-\ln[-A(J_\blacktriangle)]}, \tag{61}$$

$$\frac{J_\blacktriangledown + 0.5}{J_\blacktriangledown - 2J_\blacktriangledown^2} = \mu\sqrt{-\ln[A(J_\blacktriangledown)]}, \tag{62}$$

$$\Delta_\blacktriangle = -\frac{4}{\mu}\sqrt{-\ln[-A(J_\blacktriangle)]} - 2J_\blacktriangle + 1, \tag{63}$$

$$\Delta_\blacktriangledown = \frac{4}{\mu}\sqrt{-\ln[A(J_\blacktriangledown)]} - 2J_\blacktriangledown + 1. \tag{64}$$

Equations (61) and (62) are transcendental equations, whose solutions exist only for certain combinations of the parameters F and μ. For example, in the case of $F=0.005$, hysteresis points exist for $\mu=45$, but not for $\mu=15$ (Fig. 11). In the case of hysteresis, the behavior of a gyrotron is very interesting. Suppose that we begin to increase Δ coming from the left-hand side of Fig. 11. The oscillations would begin at $\Delta_\blacktriangle=-0.173$ and break down at $\Delta_*=0.327$. However, if we begin to decrease Δ coming from the right-hand side, the oscillations would start at $\Delta_\blacktriangledown=0.172$ and break down at $\Delta_*=-0.486$. Such related hysteresis phenomena have been studied in Ref. 18. It should be emphasized that this effect is related to the existence of the regions of soft and hard self-excitation regions in gyrotrons (see Fig. 4A in Ref. 5). For small values of F and μ we are in the soft self-excitation region (no hysteresis), for small F but large μ we are in the hard self-excitation region (hysteresis expected).

The value range of Δ which corresponds to a significant difference between the extreme action values and the initial action J_0 is directly related to the range of Δ which results in significant change in the average (with respect to initial angles) electron action at the output. Using Eq. (51), we can obtain the efficiency as a function of Δ, for the case of a beam with single action value for all electrons $J_0=0.5$, as shown in Figs. 12(a) and 12(b). Negative values of Δ result in average increasing of the action value, which correspond to the case where the rf field provides energy for the electron beam, and the gyrotron operation is reversed. The effect of a varying mismatch is a decreased efficiency, as shown in Fig. 12(b).

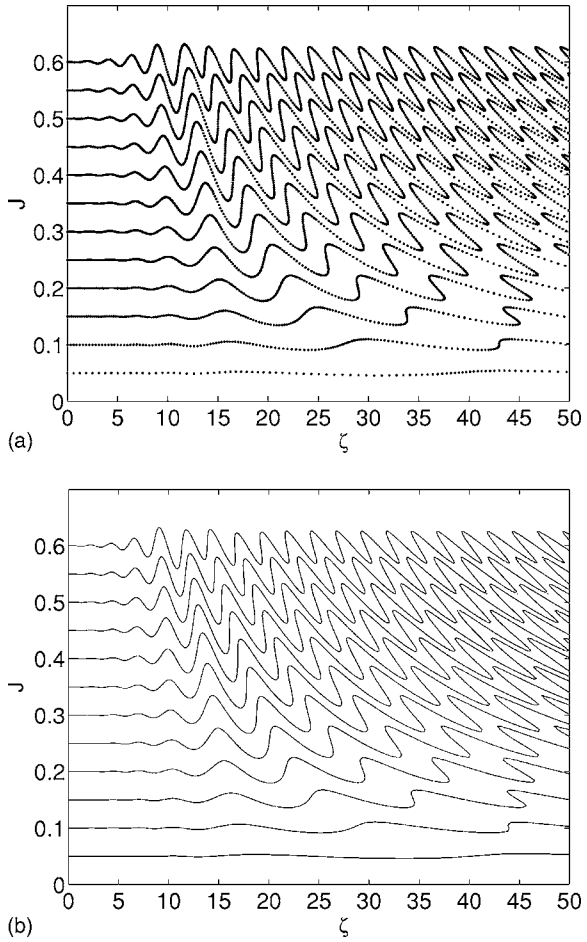

FIG. 8. Varying frequency mismatch. (a) Numerically and (b) analytically [Eqs. (20) and (21)] obtained Poincaré surface of section $\Sigma^{\theta_0=0}$. Parameter set: $F=0.01$, $\Delta=0.5$, $\mu=15$, $n=2$, $\delta^{(1)}=-0.05$.

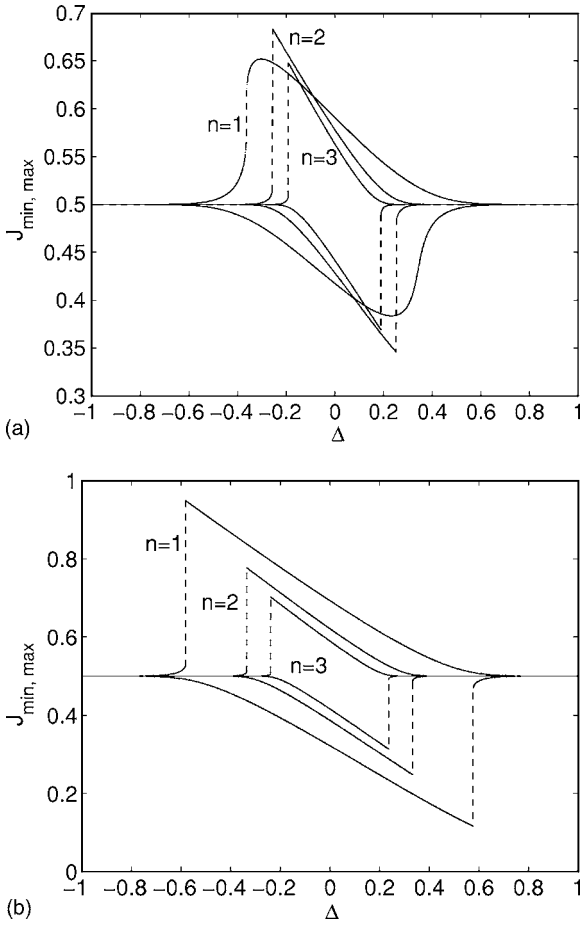

FIG. 9. Extreme output action values [Eq. (22)] for an initial action $J_0=0.5$. Parameter sets: $F=0.01$ (a), 0.1 (b), $\mu=15$, $n=1,2,3$.

B. Interaction with multiple rf modes

In the case of multiple modes the phase space of the system and the Poincaré surfaces of section consist of resonant areas corresponding to each rf mode. Depending on their position and width, these resonant areas may be well separated, weakly, or strongly overlapping. This structure of the phase-space topology is analogous to the well-studied case of multiple resonances in periodic systems, where the perturbation field has a discrete spectrum. In the case under consideration, the position of each resonance depends on the frequency mismatch (Δ) of the corresponding rf field, while its width depends on the resonator length (μ), the harmonic number (n), and the coupling factor (F).

In order to study the features of electron interaction with multiple rf modes, we focus on the case of two rf modes being in resonance with the same or different harmonic of the electron cyclotron frequency. The numerical results are accompanied with analytically obtained Poincaré surfaces of section, which can describe the structure of the phase space. First, we consider two rf modes having $n_1=1$ and $n_2=2$, respectively. The normalized resonator length is $\mu=45$, the coupling factors are $F_1=F_2=0.01$ (the same values of F_s will be used for all the following cases), and the frequency mismatches are $\Delta_1=0.7$ and $\Delta_2=0.3$. As shown in Fig. 13, the two resonant areas are centered around $(1-\Delta_s)/2=0.15,0.35(s=1,2)$ and they weakly overlap. A higher difference between the frequency mismatches, corresponding to $\Delta_1=0.7$ and $\Delta_2=0$, results in well-separated resonant areas, as shown in Fig. 14. In this case an electron beam with a given initial action value can significantly interact with just one of the two rf fields. However, for a reduced resonator length μ the width of the resonant areas increases so that the two resonances may be adjacent or overlapping, for a given set of frequency mismatches (Δ_1,Δ_2). Also, since the resonance width is decreased with the harmonic number (n), stronger overlap is expected to occur for the case where both rf modes are in resonance with the first harmonic of the cyclotron frequency $(n_1=n_2=1)$.

VI. CONCLUSIONS

In this work, electron dynamics in gyrotron resonators have been studied, by utilizing the canonical perturbation method, in order to construct approximate invariants of the motion for the nonintegrable, aperiodic Hamiltonian system, which describes the electron motion. The approximate invariants, corresponding to KAM curves, analytically provide accurate information about the strongly inhomogeneous structure of the phase space. The structure of the phase space consists of resonant areas of strong interactions, each one

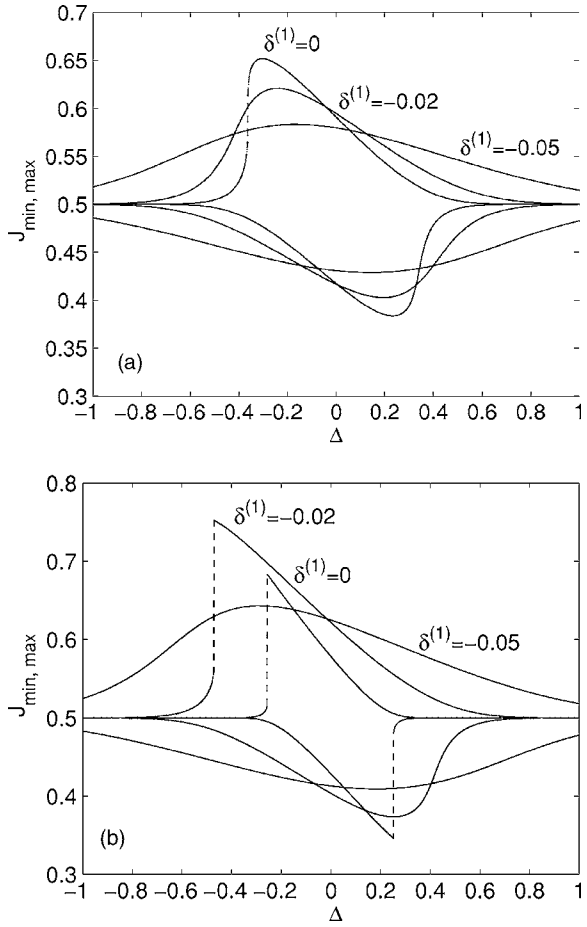

FIG. 10. Varying frequency mismatch. Extreme output action values [Eq. (22)] for an initial action $J_0=0.5$. Parameter sets: $F=0.01$, $\mu=15$, $n=1$, (a), 2 (b), $\delta^{(1)}=0,-0.02,-0.05$.

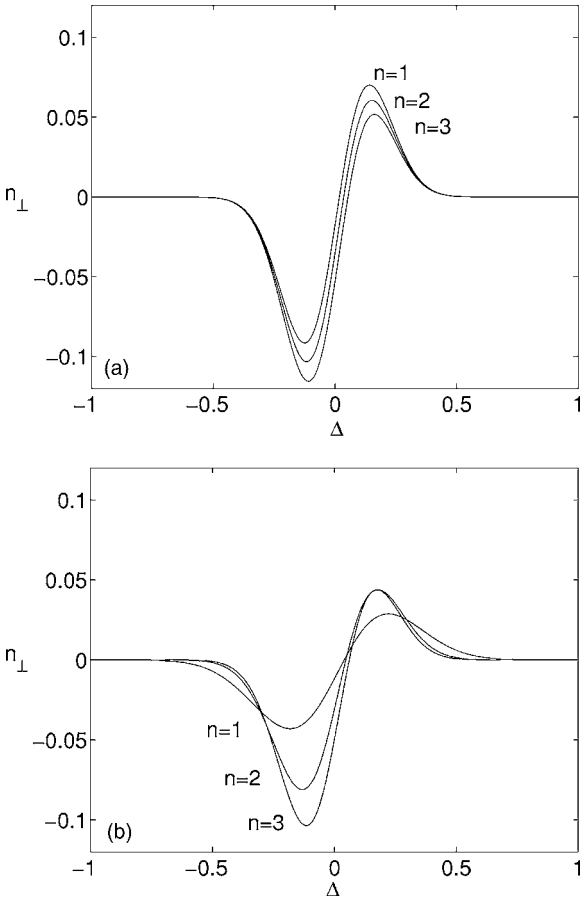

FIG. 12. Efficiency plots [Eq. (51)]. (a) Constant frequency mismatch. Parameter set: $F=0.01$, $\mu n=15$, $n=1,2,3$. (b) Varying frequency mismatch. Parameter set: $F=0.01$, $\mu n=15$, $n=1,2,3$, $\delta^{(1)}=-0.02$.

corresponding to a rf mode which is present in the cavity. The phase space is analyzed via appropriate Poincaré surfaces of section. Using the approximate invariants, the electron energy spectrum, at the output of the cavity, can also be calculated. The hysteresis effects occurring in gyrotron resonators are shown to be succesfully recovered in terms of simple analytic expressions, involving the parameters of interest. Moreover, the results of the CPM have been used in order to obtain approximate solutions of the Vlasov equation and electron distribution functions. The latter describe the collective behavior of the electron beam and can be used in order to obtain certain useful quantities, such as the efficiency, for a given initial electron distribution.

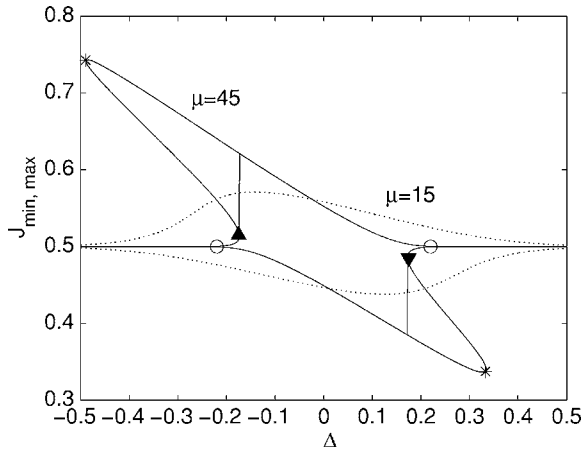

FIG. 11. Case of multiple roots of Eq. (22) related to hysteresis effects. Parameter set: $F=0.005$, $\mu=15,45$, $n=1$, $\delta^{(1)}=0$.

The aforementioned results have been, first, applied to the case of electron interaction with a single rf mode being in resonance with any harmonic of the electron cyclotron frequency. The position and the width of the corresponding resonant area of the phase space and their dependency on the frequency mismatch and the resonator length have been studied. The case of magnetic-field tapering resulting in a varying frequency mismatch has also been included, and its effect on the resonant area has been shown. Efficiency calculations have been given in terms of the approximate distribution function, resulting in expressions for the case of Dirac or Gaussian initial transverse momentum (action) distributions. It is worth mentioning that the approximate distribution functions can also be used for the calculation of any other collective quantity of the electron beam.

Also, the case of beam interaction with multiple rf modes has been investigated for the characteristic cases of two rf modes being in resonance with the same or different

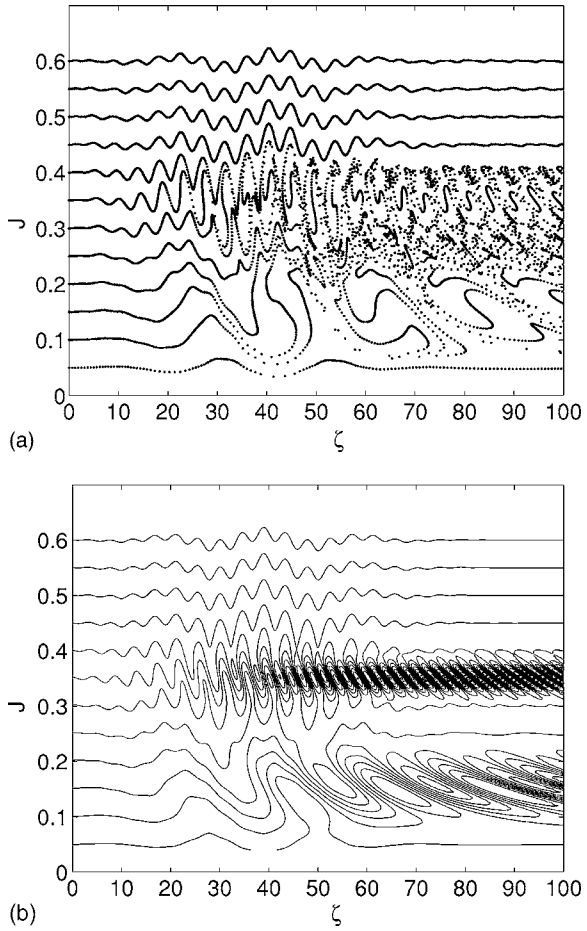

FIG. 13. (a) Numerically and (b) analytically [Eqs. (20) and (21)] obtained Poincaré surface of section $\Sigma^{\theta_0=0}$ for two modes being in resonance with different harmonics of the electron cyclotron frequency. Parameter set: $(n_1,n_2)=(1,2)$, $(F_1,F_2)=(0.01,0.01)$, $(\mu_1,\mu_2)=(45,45)$, $(\Delta_1,\Delta_2)=(0.7,0.3)$.

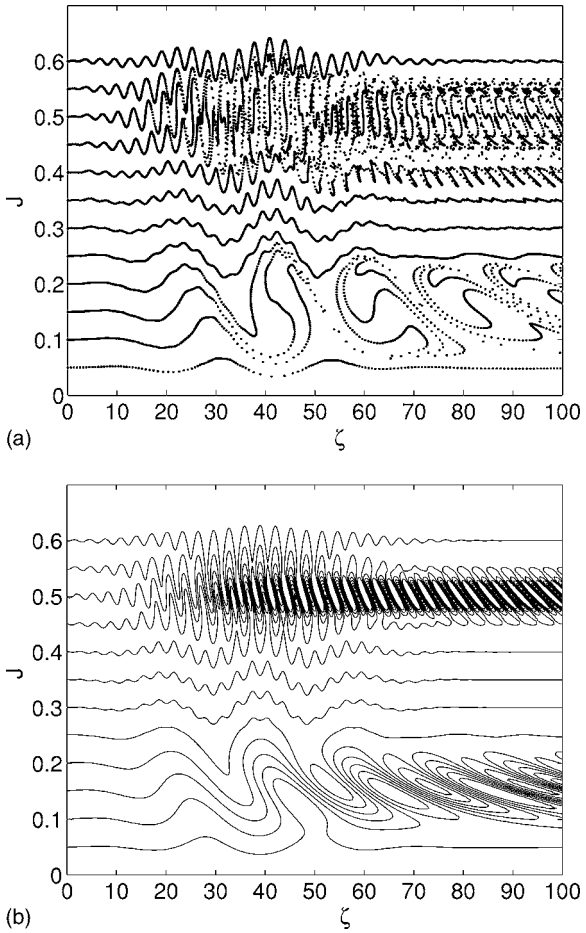

FIG. 14. (a) Numerically and (b) analytically [Eqs. (20) and (21)] obtained Poincaré surface of section $\Sigma^{\theta_0=0}$ for two modes being in resonance with different harmonics of the electron cyclotron frequency. Parameter set: $(n_1,n_2)=(1,2)$, $(F_1,F_2)=(0.01,0.01)$, $(\mu_1,\mu_2)=(45,45)$, $(\Delta_1,\Delta_2)=(0.7,0)$.

harmonics of the electron cyclotron frequency. Depending on the specific parameter choice, the two resonant areas of the phase space are shown to be well separated, neighboring, weakly, or strongly overlapping. The resonant area overlap results in the fact that certain initial action values are strongly affected by both resonances. Although, the CPM can also proceed to higher order, it is shown that even low-order calculations provide analytical results which are in good agreement with numerical results, and give a clear physical insight to the mechanism governing the beam interaction with the rf field inside the gyrotron cavity.

Finally, it should be stressed that in this work the emphasis was put on various mathematical aspects of the Hamiltonian approach to studying electron dynamics in gyrotron resonators. Attempts to interpret the results in terms of parameters of some real gyrotrons lie beyond the scope of this work. Some specific examples can be found in Ref. 19 where the Hamiltonian formalism was used for developing the nonlinear, fully relativistic, multimode theory of gyro-traveling-wave amplifiers with tapered magnetic fields and nonuniform waveguides.

ACKNOWLEDGMENT

This work was supported in part by the European Fusion Programme (EURATOM) and the Greek General Secretariat of Research and Technology. The sponsors do not bear any responsibility for the contents in this work.

APPENDIX: FIRST-ORDER GENERATING FUNCTION

In order to solve the linear differential equation (18) to obtain S_1, instead of using the usual Fourier series method which applies for periodic perturbation, we use the Fourier transform method so that (18) transforms to

$$i\Omega \mathbb{S}_1 + \omega_\theta(ik)\mathbb{S}_1 = 2\pi \sum_s F_s (2J)^{n_s/2} \mathbb{G}_s(\Omega)\delta(k-n_s), \quad \text{(A1)}$$

where $\theta \rightleftharpoons k$, $\zeta \rightleftharpoons \Omega$ and $\mathbb{S}_1(J,k,\Omega)$, $\mathbb{G}_s(\Omega)$ are the Fourier transforms of $S_1(J,\theta,\zeta)$ and $g_s(\zeta)$, respectively. Note that, for simplicity, we can work with the complex equation, but keep only the real part, at the final results. Solving (A1) and using the inverse Fourier transform, S_1 is obtained as follows:

$$S_1 = \sum_s F_s (2J)^{n_s/2} e^{in_s\theta} \frac{1}{2\pi} \int_{-\infty}^{+\infty} \frac{\mathbb{G}_s(\Omega)}{\Omega + n_s\omega_\theta} e^{i\Omega z} d\Omega. \quad \text{(A2)}$$

The integral

$$I_s(\omega_\theta(J), \zeta) = \frac{1}{2\pi} \int_{-\infty}^{+\infty} \frac{\mathbb{G}_s(\Omega)}{\Omega + n_s\omega_\theta} e^{i\Omega\zeta} d\Omega \quad \text{(A3)}$$

has a simple real pole at $\Omega = -n_s\omega_\theta$, and the contour of integration in the complex plane is deformed in order to bypass the real pole in a counterclockwise direction, so that the causality condition

$$\lim_{\zeta \to -\infty} S_1 = 0 \quad \text{(A4)}$$

is fulfilled. Thus, the integral can be written in the following form:

$$I_s = \frac{1}{2\pi} \left[P \int_{-\infty}^{+\infty} \frac{\mathbb{G}_s(\Omega)}{\Omega + n_s\omega_\theta} e^{i\Omega\zeta} d\Omega + i\pi \mathbb{G}_s(-n_s\omega_\theta) e^{-in_s\omega_\theta\zeta} \right], \quad \text{(A5)}$$

with P denoting the Cauchy principal value of the integral and the second term taking into account the contribution of the real pole. Identifying the first term as an inverse Fourier transform and using the frequency shift and integration properties of the Fourier transform, we have

$$I_s = e^{-in_s\omega_\theta\zeta} \int_{-\infty}^{\zeta} g_s(t) e^{in_s\omega_\theta t} dt. \quad \text{(A6)}$$

For all functions $g_s(\zeta)$ having a well-defined Fourier transform, the first-order generating function S_1 is given from Eqs. (A1) and (A6) or (A3). For the specific case of a Gaussian profile (54), the calculation of integral I_s is quite similar to the integral involved in the plasma dispersion relation.

[1] T. Idehara, S. Mitsudo, R. Pavlichenko, I. Ogawa, D. Wagner, and M. Thumm, "Development of submillimeter wave gyrotron FU series," *Proceedings of the International Workshop, Nizhny Novgorod, Russia, 1–9 August 2002* (Institute of Applied Physics, Russian Academy of Sciences, Russia, 2003), p. 116.

[2] G. G. Denisov, "Megawatt gyrotrons for fusion research. State of the art and trends of development, Strong Microwaves in Plasmas," *Proceedings of the International Workshop, Nizhny Novgorod, Russia, 1–9 August 2002* (Institute of Applied Physics, Russian Academy of Sciences, 2003), p. 29.

[3] G. Dammertz, S. Alberti, A. Arnold, E. Borie, V. Erckmann, G. Gantenbein, E. Giguet, R. Heidinger, J. P. Hogge, S. Illy, W. Kasparek, K. Koppenburg, M. Kuntze, H. P. Laqua, G. LeCloarec, Y. LeGoff, W. Leonhardt, C. Lievin, R. Magne, G. Michel, G. Mueller, G. Neffe, B. Piosczyk, M. Schmid, K. Schwoerer, M. K. Thumm, and M. Q. Tran, IEEE Trans. Plasma Sci. **30**, 808 (2002).

[4] B. Piosczyk, G. Dammertz, O. Dumbrajs, O. Drumm, S. Illy, J. Jin, and M. Thumm, IEEE Trans. Plasma Sci. **32**, 413 (2004).

[5] G. S. Nusinovich, *Introduction to the Physics of Gyrotrons* (The Johns Hopkins University Press, Baltimore, 2004).

[6] M. I. Airila and O. Dumbrajs, Phys. Plasmas **8**, 1358 (2001).

[7] M. I. Airila, O. Dumbrajs, A. Reinfelds, and U. Strautins, Phys. Plasmas **8**, 4608 (2001).

[8] A. J. Lichtenberg and M. A. Lieberman, *Regular and Chaotic Dynamics* (Springer-Verlag, New York, 1992).

[9] O. Dumbrajs, R. Meyer-Spasche, and A. Reinfelds, IEEE Trans. Plasma Sci. **26**, 846 (1998).

[10] M. I. Airila, O. Dumbrajs, A. Reinfelds, and D. Teychenne, Int. J. Infrared Millim. Waves **21**, 1759 (2000).

[11] O. Dumbrajs and D. Teychenne, J. Commun. Technol. Electron. **47**, 1364 (2002).

[12] Y. Kominis, O. Dumbrajs, K. A. Avramides, K. Hizanidis, and J. L. Vomvoridis, Phys. Plasmas **12**, 043104 (2005).

[13] G. S. Nusinovich, R. Ngogang, T. M. Antonsen, and V. L. Granatstein, Phys. Rev. Lett. **93**, 055101 (2004).

[14] A. Deprit, Celest. Mech. **1**, 12 (1969).

[15] P. E. Latham, S. M. Miller, and C. D. Striffler, Phys. Rev. A **45**, 1197 (1992).

[16] B. G. Danly and R. J. Temkin, Phys. Fluids **29**, 561 (1986).

[17] G. S. Nusinovich, Int. J. Electron. **64**, 127 (1988).

[18] O. Dumbrajs, T. Idehara, Y. Iwata, S. Mitsudo, I. Ogawa, and B. Piosczyk, Phys. Plasmas **10**, 1183 (2003).

[19] P. E. Latham and G. S. Nusinovich, Phys. Plasmas **2**, 3494 (1995).